Friction **10**(2): 209–216 (2022)
https://doi.org/10.1007/s40544-020-0418-8
ISSN 2223-7690
CN 10-1237/TH
RESEARCH ARTICLE

Superlubricity of molybdenum disulfide subjected to large compressive strains

Shengcong WU, Zhisen MENG, Xiaoma TAO, Zhao WANG*

Guangxi Key Laboratory for Relativistic Astrophysics, Department of Physics, Guangxi University, Nanning 530004, China

Received: 17 December 2019 / Revised: 08 May 2020 / Accepted: 12 June 2020

Abstract: The friction between a molybdenum disulphide (MoS_2) nanoflake and a MoS_2 substrate was analyzed using a modified Tomlinson model based on atomistic force fields. The calculations performed in the study suggest that large deformations in the substrate can induce a dramatic decrease in the friction between the nanoflake and the substrate to produce the so-called superlubricity. The coefficient of friction decreases by 1–4 orders of magnitude when a high strain exceeding 0.1 is applied. This friction reduction is strongly anisotropic. For example, the reduction is most pronounced in the compressive regime when the nanoflake slides along the zigzag crystalline direction of the substrate. In other sliding directions, the coefficient of friction will reduce to its lowest value either when a high tensile strain is applied along the zigzag direction or when a high compressive strain is applied along the armchair direction. This anisotropy is correlated with the atomic configurations of MoS_2.

Keywords: superlubricity; friction; molybdenum disulfide; strain

1 Introduction

In mechanical systems, friction is unavoidable. Friction increases energy consumption and wear, and reduces the life of device components [1, 2]. These problems caused by friction are particularly important in nanometer-sized devices and machines because of the high surface-to-volume ratio of nanostructures. Two-dimensional (2D) materials [3–5], such as graphene [6] and molybdenum disulfide (MoS_2) [7, 8] can considerably reduce the wear and friction in mechanical systems, owing to their chemical inertness [9–12], high strength [13], and peculiar structure [14]. For example, Kawai et al. discovered ultra-low friction between graphene nanoribbons and an Au surface [15]. Li et al. found that the coefficient of kinetic friction falls below 10^{-4} when a single-layer MoS_2 flake slides on a MoS_2 surface [16]. Such ultra-low friction state induced by an incommensurate interface registry is called structural superlubricity [17–20].

However, achieving robust superlubricity using 2D materials is challenging. Filippov et al. [21] demonstrated the instability of superlubricity in graphene caused by the reorientation of contacting layers at the interface. Bonelli et al. [22] reported that the rotation of graphene flakes can change the incommensurate registry of the interface, causing high friction. To achieve steady superlubricity, Leven et al. [23] proposed the use of a graphene–boron nitride (BN) for stabilizing the incommensurate registry of the lattice using the registry index concept. Wang et al. predicted, using molecular dynamics simulations, that stable superlubricity can be achieved by stretching the graphene substrate on which the graphene flake slides [24]. It was shown that robust superlubricity can be achieved in 2D nanostructures via strain engineering.

* Corresponding author: Zhao WANG, E-mail: zw@gxu.edu.cn

Lin et al. [25] reported that the friction between a graphene flake and a graphene substrate is almost insensitive to small compressive strains. The effect of high strains is unclear, and thus, requires exploration because nanostructures are known to sustain larger deformations than their bulk counterparts [26–29]. In this study, we used Tomlinson-type simulations [30–34] based on atomistic force fields to study the friction between a MoS_2 flake and a MoS_2 substrate. The substrate was subjected to large deformations, causing superlubric friction.

2 Methods

In our simulations, a hexagonal MoS_2 flake composed of 81 atoms was made to slide atop an infinite MoS_2 substrate. As shown in Fig. 1, the flake was connected with three springs, which were used to monitor the motion of the flake. The deformation (either compressive or tensile) was applied to the substrate by changing the coordinates of the atoms for a Poisson ratio of 0.267 [35]. In accordance with the deformation, the periodic length and width of the simulation box were adjusted from L_0 and W_0 to L and W, respectively, for completely relaxing the pressure on the substrate along the x-and y-axes, respectively. The in-plane strain is given by $\varepsilon_x = (L–L_0)/L_0$ or $\varepsilon_y = (W–W_0)/W_0$, depending on the direction of the applied deformation. A negative deformation represents a compressive strain while a positive one represents a tensile strain. The applied strain was below the previously reported elongation limit of the material by a value between –0.2 and 0.2 [36]. Buckling occurs when large compressive strains are applied on free-standing MoS_2 [37]. Although buckling was ignored in the simulation setup we used, Moiré template strain patterning methods can be used, if necessary, to reduce the buckling [38, 39]. The sliding direction is represented by the angle ω between the direction of the movement of the MoS_2 flake and the x-axis (Fig. 1).

The interaction between the flake and the substrate was here considered at the atomistic level. It consisted of two parts: van der Waals (vdW) and electrostatic (elec) interactions. Because the two contacting bodies

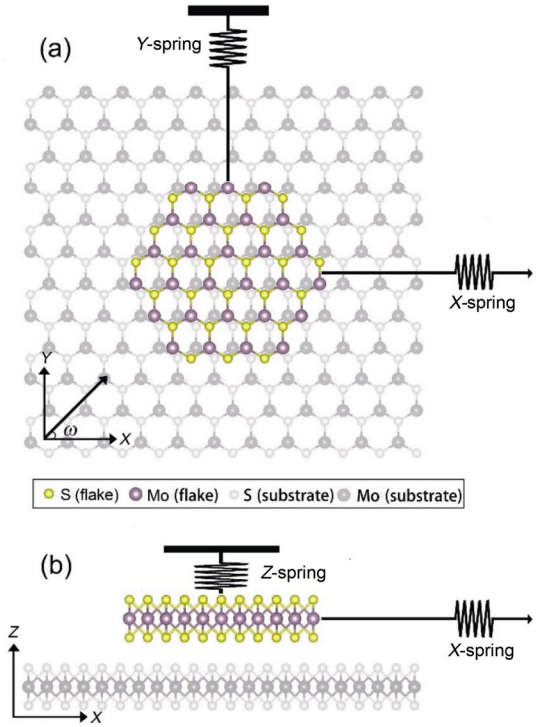

Fig. 1 Model setup. (a) Top view and (b) side view of a hexagonal MoS_2 flake (orthogonally connected with three springs) atop a MoS_2 monolayer substrate.

were both assumed to be rigid, the total interaction potential ccould be written as

$$E^{\text{int}} = \sum_{i=1}^{N_1}\sum_{j=1}^{N_2} E_{ij}^{\text{vdw}} + \sum_{i=1}^{N_1}\sum_{j=1}^{N_2} E_{ij}^{\text{elec}} \tag{1}$$

where i and j are the index of atoms in the flake and substrate, respectively. The Lennard–Jones force field [40] was as follows:

$$E_{ij}^{\text{vdw}} = 4\epsilon\left[\left(\frac{\sigma}{r_{ij}}\right)^{12} + \left(\frac{\sigma}{r_{ij}}\right)^{6}\right] \tag{2}$$

with a potential well depth of 0.586, 2.800, and 13.860 meV and an equilibrium distance of 0.420, 0.367, and 0.313 nm for Mo–Mo, Mo–S, and S–S interactions, respectively [41]. The cutoff radius for the vdW potential was set to be 1.0 nm.

The electrostatic potential is was calculated using the pairwise Coulomb function given below.

$$E_{ij}^{\text{elec}} = C\frac{q_i q_j}{\epsilon_0 r_{ij}} \tag{3}$$

where C is the Coulomb constant. q = 0.76e and

−0.38*e* are the effective partial charges for Mo and S, respectively [42, 43]. The cutoff radius for the elec potential was set to be 3.0 nm.

The total potential energy of the system included the total interaction potential and the elastic potential stored in the springs as indicated below.

$$E^{total}\left(\boldsymbol{R}^{f},\boldsymbol{R}^{s}\right)=E^{int}+\frac{1}{2}k_{x}\left(R_{x}^{f}-R_{x}^{s}\right)^{2}+\frac{1}{2}k_{y}\left(R_{y}^{f}-R_{y}^{s}\right)^{2}+\frac{1}{2}k_{z}\left(R_{z}^{f}-R_{z}^{s}\right)^{2} \tag{4}$$

where $\boldsymbol{R}^{f}$ is the vector pointing to the center of the mass of the MoS_2 flake and $\boldsymbol{R}^{s}$ is that pointing to the root of the spring. The rigidity constants of the *x*- and *y*-springs were set to $k_x = k_y = 55$ N/m, based on experimentally reported values [44, 45]. The *Z*-spring was used to maintain a constant normal load. In the Tomlinson model, stick–slip instability and the associated energy dissipation critically depend on the force constant of the loading springs. As shown in Fig. S1 in the Electronic Supplementary Material (ESM), the coefficient of friction decreases as the rigidity constant increases and becomes zero when the rigidity constant is large. The stick–slip behavior was active for the rigidity constant used.

In our simulation, the MoS_2 flake slid in discrete steps of 0.001 nm. Its position was spontaneously adjusted at each step by the springs for a nearby local energy minimum [31, 44, 46]. The friction force *F* was calculated as the average force acting on the flake against the sliding direction during the last 70% of the simulation steps (in a total sliding distance of 10 nm) [31]. To determine the influence of the initial position of the flake, we simulated 100 different initial positions for the flake. As a benchmark, we calculated the friction force as a function of the normal load without any applied strain, as shown in Fig. S2 in the ESM. The friction linearly increased with the load at a relatively large load, endorsing past experimental observations [47–49].

3 Results and discussion

Figure 2 shows the friction force as a function of the sliding distance of the flake. A typical stick–slip behavior is observable even with high tensile strain (Fig. 2(a)). This type of behavior has been observed in many nanoscale friction experiments [17, 44]. However, the stick–slip motion appears to have been significantly hindered by the high compressive strain applied to the substrate. This is because, as Fig. 2(b) depicts, under a high compressive strain, the abrupt jumps in the curves of the friction force disappear, signifying the achievement of a stable superlubric state.

To confirm this, we computed the coefficient of friction μ and plotted it as a function of the applied strain (Fig. 3). As can be seen in Fig. 3, when no strain is applied, $\mu = 0.23$ for the given normal force. Under a small tensile or compressive strain, μ starts to decrease, confirming the results of previous studies [24, 25]. When the magnitude of the applied strain exceeds 0.1, μ dramatically decreases, particularly in the case of compressive strain ($\varepsilon < 0$). For example, μ decreases by 4 orders of magnitude when a compressive strain of 0.2 is applied to the substrate in either the *x*- or *y*-directions, as shown in Figs. 3(a) and 3(b), respectively, under a normal force $F_n = 8.1$ nN.

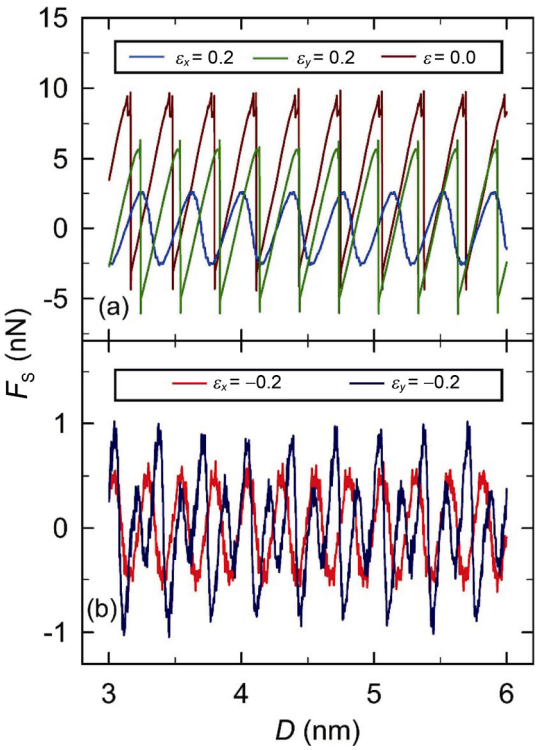

Fig. 2 Instantaneous force acting on the MoS_2 flake vs. its sliding distance when the substrate is subjected to (a) high tensile strain and (b) high compressive strain, at a normal force F_n=16.2 nN and $\omega = 0$.

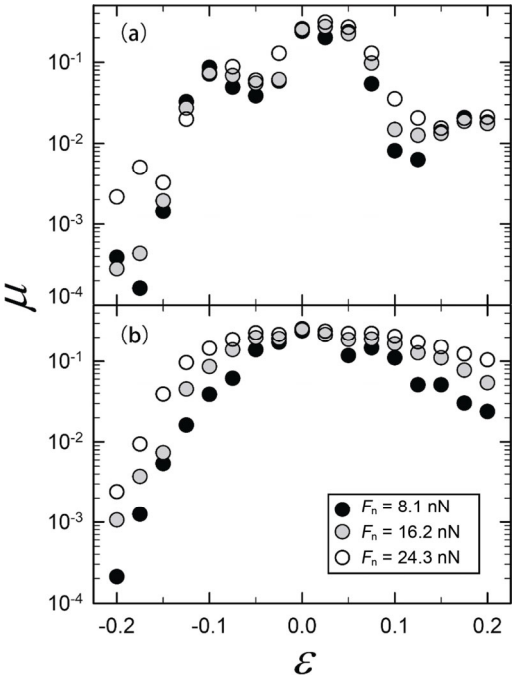

Fig. 3 Coefficient of friction vs. strain applied to the substrate along the (a) x-direction and (b) y-direction, with a constant normal force (F_n = 8.1, 16.2 or 24.3 nN) and ω = 0.

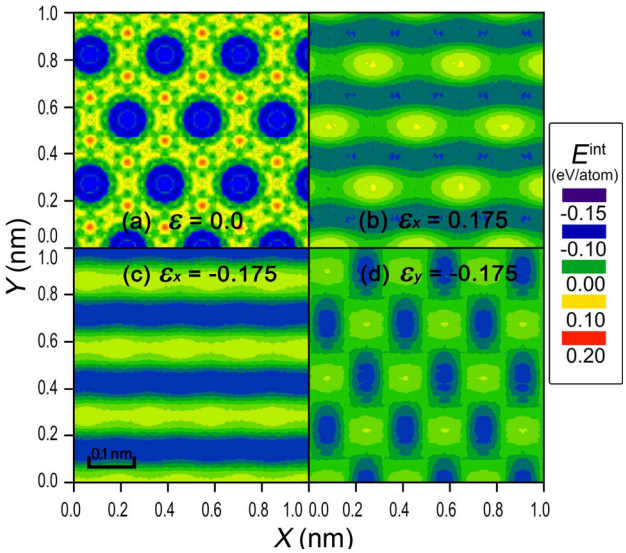

Fig. 4 Potential energy surface (PES) between the MoS_2 flake and the substrate subjected to (a) no strain, (b) ε_x = 0.175, (c) ε_x = –0.175, and (d) ε_y = –0.175.

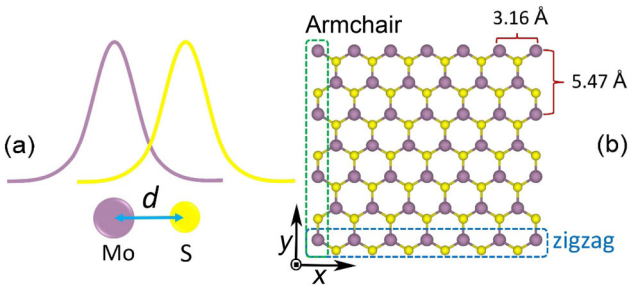

Fig. 5 (a) Schematic of the overlapping long-range interaction potential energy on two atomic sites and (b) different atom densities of MoS_2 along the armchair and zigzag directions.

The effect of high tensile strain is however less significant than that of high compressive strain, which endorses the results of Wang et al. [24].

To understand the dramatic decrease of the coefficient of friction under large strains, the potential energy surface (PES), which is strongly correlated with the friction properties of the interface [50, 51], was plotted in Fig. 4. The energy values shown were obtained by computing the total interaction potential when displacing the flake atop the substrate in discrete steps. As shown in Fig. 4, the PES has been significantly changed by the high strain applied to the substrate. The friction has to change accordingly because the principle of minimum energy makes the flake to "surf" waves on the PES along a path corresponding to the lowest energy corrugation. The energy corrugation along the x-axis reaches its minimum for ε_x = –0.175 (Fig. 4(c)), while the energy barriers in the sliding pathway reach the maximum when there is no applied strain (Fig. 4(a)).

The positive and negative strains cause different friction reductions. This anisotropy is correlated with the fact that a compressive strain will result in a shorter interatomic distance, enhancing the overlapping of the long-range interaction potential energy of the atoms, which makes the peaks in the long-range interaction potential surface to be closer, as can be seen in Fig. 5(a). Hence, the PES will be "smoother"in the case of compressive strain. By contrast, tensile strain increases the energy surface corrugation with an increased interatomic distance, causing higher friction [24]. This effect can be seen by comparing the energy profile in Fig. 4(b) with that in Fig. 4(c).

The difference between the friction resulting from the straining of the substrate in the x-direction and the corresponding friction in the y-direction, which is another aspect of the anisotropy of the friction reduction effect, is correlated with the difference in the atom densities of MoS_2 along different crystalline directions. As shown in Fig. 5(b), the atom density

along the zigzag direction is higher than that along the armchair direction. Thus, when a strain is applied to the substrate, the induced lattice mismatch between the two layers at the interface can be higher for the strain along the zigzag direction. An enhanced lattice mismatch is known to cause higher friction [31].

The results mentioned are for the flake sliding along the *x*-axis. To consider a more general scenario, we simulated the sliding of the flake in different directions. The coefficient of friction was computed for different applied strains (Fig. 6). In all sliding directions, μ had the highest value for the pristine substrate under no strain. By contrast, μ generally had the lowest value when a tensile strain of 0.15 was applied along the *x-axis*, as shown in Fig. 6(a), or when a compressive strain of –0.15 was applied along the *y-axis*, as shown in Fig. 6(b). The sliding direction corresponding to the minimum μ changes with the applied strain. For example, when $\omega = 0$ or π for $\varepsilon_x = -0.15$, while $\omega = \pi/6$ or $5\pi/6$ for $\varepsilon_x = 0.05$ or $\varepsilon_x = -0.05$, as shown in Fig. 6(a). For the strain applied in the *y*-direction, the sliding direction corresponding to the lowest friction is $\omega = \pi/6$ or $5\pi/6$ for $\varepsilon_y = -0.15$, while it is $\omega = \pi/3$ or $2\pi/3$ for $\varepsilon_y = 0.15$.

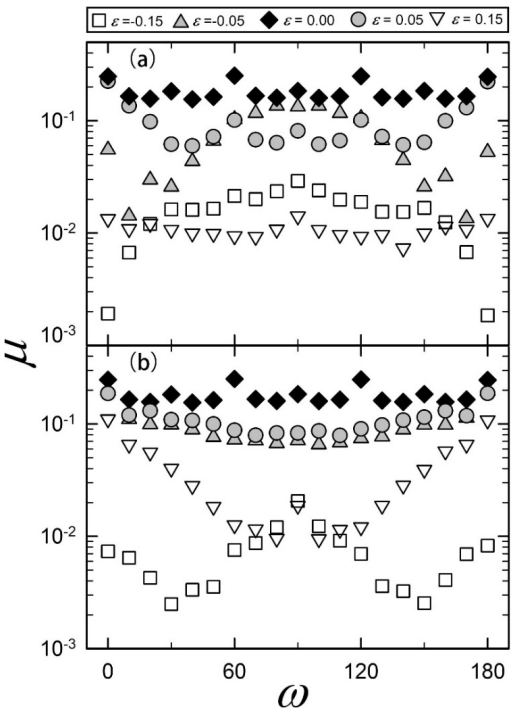

Fig. 6 Coefficient of friction computed for different sliding directions with different strains applied to the substrate along the (a) *x*-axis and (b) *y*-axis.

We also calculated the coefficient of friction for three different flake sizes (Fig. 7). As Fig. 7 shows, μ increases as the size of the flake increases with no applied strain. However, μ decreases with increasing flake size with a compressive strain of –0.175 applied in the *y*-direction or with a tensile strain of 0.175 applied in the *x*-direction. This result is in line with the findings of Leven et al. [23] that overall registry index corrugation monotonously reduces with the increase in the flake size at the interface between graphene and hexagonal boron nitride. As an exception, when a compressive strain of –0.175 was applied along the *x*-direction, the μ of the largest flake (N = 144) was less than that of the smallest flake (N = 36), and the μ of the flakes of intermediate size had the lowest value.

4 Summary

We simulated the sliding of a rigid MoS_2 flake on a strained MoS_2 substrate using a modified Tomlinson model combined with atomistic force fields. The simulations indicate that a large deformation of the substrate can induce a dramatic decrease in the friction coefficient causing the so-called superlubricity. For example, the coefficient of friction decreased by 4 orders of magnitude when a high compressive

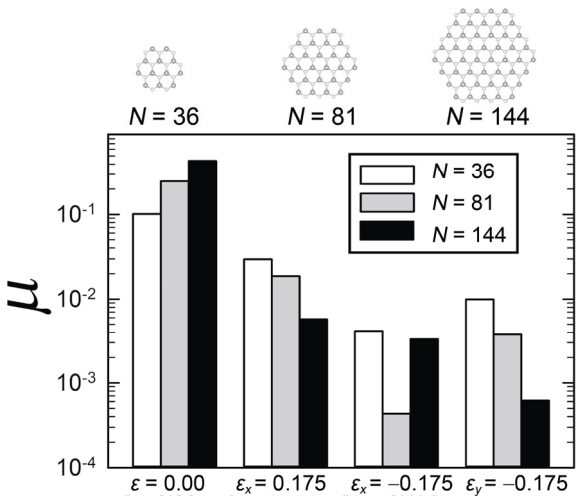

Fig. 7 Coefficient of friction computed with different sizes of the flake (number of atoms N = 36, 81, or 144), with a constant normal force of 16.2 nN and ω= 0 at different strain levels.

strain of 0.2 was applied to a pristine substrate. This friction reduction effect is found to be highly anisotropic. In most sliding directions, the coefficient of friction is, in general, the lowest when a high tensile strain is applied along the x-direction, or with a high compressive strain applied along the y-direction. This anisotropic effect is correlated with the atomic configurations of MoS_2 as explained by the strain-induced change in the PES between the MoS_2 flake and the substrate. The simulations were expanded to represent more general scenarios by making the flake to slide in different directions. The sliding direction corresponding to the lowest coefficient of friction depended on the magnitude of the applied strain.

Acknowledgements

Partial financial supports from the National Natural Science Foundation of China (No. 11964002), the Guangxi Science Foundation (No. 2018GXNSFAA-138179), and the Scientific Research Foundation of Guangxi University (No. XTZ160532) are acknowledged.

Electronic Supplementary Material: Supplementary material is available in the online version of this article at https://doi.org/10.1007/s40544-020-0418-8.

References

[1] Holmberg K, Andersson P, ErdemirA. Global energy consumption due to friction in passenger cars. *Tribol Int* **47**: 221–234 (2012)

[2] Holmberg K, Erdemir A. Influence of tribology on global energy consumption, costs and emissions. *Friction* **5**(3): 263–284 (2017)

[3] Guo W, Yin J, Qiu H, Guo Y, Wu H, Xue M. Friction of low-dimensional nanomaterial systems. *Friction* **2**(3): 209–225 (2014)

[4] Liu L, Zhou M, Jian L, Li L, Mo Y, Su G, Li X, Zhu H, Tian Y. Recent advances in friction and lubrication of graphene and other 2D materials: Mechanisms and applications. *Friction* **7**(3): 199–216 (2019)

[5] Wang W, Xie G, Luo J. Black phosphorus as a new lubricant. *Friction* **6**(1): 116–142 (2018)

[6] Fan X, Xue Q, Wang L. Carbon-based solid-liquid lubricating coatings for space applications—A review. *Friction* **3**(3): 191–207 (2015)

[7] Ky D L C, Khac B C T, Le C T, Kim Y S, Chung K H. Friction characteristics of mechanically exfoliated and CVD-grown single-layer MoS_2. *Friction* **6**(4): 395–406 (2018)

[8] Nian J, Chen L, Guo Z, Liu W. Computational investigation of the lubrication behaviors of dioxides and disulfides of molybdenum and tungsten in vacuum. *Friction* **5**(1): 23–31 (2017)

[9] Hu K H, Hu X G, Sun X J. Morphological effect of MoS_2 nanoparticles on catalytic oxidation and vacuum lubrication. *Appl Surf Sci* **256**(8): 2517–2523 (2010)

[10] Chu X, Yousaf A, Li D, Tang A, DebnathA, Ma D, Green A, Santos E, Wang Q. Direct covalent chemical functionalization of unmodified two-dimensional molybdenum disulfide. *Chem Mater* **30**(6): 2112–2128 (2018)

[11] Wang Z. Lubricity of graphene on rough Au surfaces. *J Phys D: Appl Phys* **51**(43): 435301 (2018)

[12] Cai M, Yu Q, Zhou F, Liu W. Physicochemistry aspects on frictional interfaces. *Friction* **5**(4): 361–382 (2017)

[13] Bertolazzi S, Brivio J, Kis A. Stretching and breaking of ultrathin MoS_2. *ACS Nano* **5**(12): 9703–9709 (2011)

[14] Lee C, Yan H, Brus L E, Heinz T F, Hone J, Ryu S. Anomalous lattice vibrations of single-and few-layer MoS_2. *ACS Nano* **4**(5): 2695–2700 (2010)

[15] Kawai S, Benassi A, Gnecco E, Sode H, Pawlak R, Feng X, Mullen K, Passerone D, Pignedoli C, Ruffieux P, et al. Superlubricity of graphene nanoribbons on gold surfaces. *Science* **351**(6276): 957–961 (2016)

[16] Li H, Wang J, Gao S, Chen Q, Peng L, Liu K, Wei X. Superlubricity between MoS_2 monolayers. *Adv Mater*

29(27): 1701474 (2017)
[17] Dienwiebel M, Verhoeven G S, Pradeep N, Frenken J W, Heimberg J A, Zandbergen H W. Superlubricity of graphite. *Phys Rev Lett* **92**(12): 126101 (2004)
[18] Zheng Q, Liu Z. Experimental advances in superlubricity. *Friction* **2**(2): 182–192 (2014)
[19] Dietzel D, Schwarz U D, Schirmeisen A. Nanotribological studies using nanoparticle manipulation: Principles and application to structural lubricity. *Friction* **2**(2): 114–139 (2014)
[20] Meyer E, Gnecco E. Superlubricity on the nanometer scale. *Friction* **2**(2): 106–113 (2014)
[21] Filippov A E, Dienwiebel M, Frenken J W, Klafter J, Urbakh M. Torque and twist against superlubricity. *Phys Rev Lett* **100**(4): 046102 (2008)
[22] Bonelli F, Manini N, Cadelano E, Colombo L. Atomistic simulations of the sliding friction of graphene flakes. *Eur Phys J B* **70**(4): 449–459 (2009)
[23] Leven I, Krepel D, Shemesh O, Hod O. Robust superlubricity in graphene/*h*-BN heterojunctions. *J Phys Chem Lett* **4**(1): 115–120 (2013)
[24] Wang K, Ouyang W, Cao W, Ma M, Zheng Q. Robust superlubricity by strain engineering. *Nanoscale* **11**(5): 2186–2193 (2019)
[25] Lin X, Zhang H, Guo Z, Chang T. Strain engineering of friction between graphene layers. *Tribol Int* **131**: 686–693 (2019)
[26] Wang Z, Philippe L. Deformation of doubly clamped single-walled carbon nanotubes in an electrostatic field. *Phys Rev Lett* **102**(21): 215501 (2009)
[27] Guo W, Wang Z, Li J. Diffusive versus displacive contact plasticity of nanoscale asperities: Temperature- and velocity-dependent strongest size. *Nano Lett* **15**(10): 6582–6585 (2015)
[28] Roldán R, Castellanos-Gomez A, Cappelluti E, Guinea F. Strain engineering in semiconducting two-dimensional crystals. *J Phys: Condens Matter* **27**(31): 313201 (2015)
[29] Wang Z, Mook W M, Niederberger C, Ghisleni R, Philippe L, Michler J. Compression of nanowires using a flat indenter: diametrical elasticity measurement. *Nano Lett* **12**(5): 2289–2293 (2012)
[30] Tomlinson G A. CVI A molecular theory of friction. *The London, Edinburgh, and Dublin Philosophical Magazine and Journal of Science* **7**(46): 905–939 (1929)
[31] Verhoeven G S, Dienwiebel M, Frenken J W. Model calculations of superlubricity of graphite. *Phys Rev B* **70**(16): 165418 (2004)
[32] Hirano M. Atomistics of superlubricity. *Friction* **2**(2): 95–105 (2014)
[33] Hu Y Z, Ma T B, Wang H. Energy dissipation in atomic-scale friction. *Friction* **1**(1): 24–40 (2013)
[34] Wang Z J, Ma T B, Hu Y Z, Xu L, Wang H. Energy dissipation of atomic-scale friction based on one-dimensional Prandtl-Tomlinson model. *Friction* **3**(2): 170–182 (2015)
[35] Xiong S, Cao G. Molecular dynamics simulations of mechanical properties of monolayer MoS_2. *Nanotechnology* **26**(18): 185705 (2015)
[36] Li J, Medhekar N V, Shenoy V B. Bonding charge density and ultimate strength of monolayer transition metal dichalcogenides. *J Phys Chem C* **117**(30): 15842–15848 (2013)
[37] Wang Z, Devel M. Periodic ripples in suspended graphene. *Phys Rev B* **83**(12): 125422 (2011)
[38] Zhu S, Johnson H T. Moiré-templated strain patterning in transition-metal dichalcogenides and application in twisted bilayer MoS_2. *Nanoscale* **10**(44): 20689–20701 (2018)
[39] Zhang C, Song J, Yang Q. Periodic buckling patterns of graphene/hexagonal boron nitride heterostructure. *Nanotechnology* **25**(44): 445401 (2014)
[40] Bortoleto E M, Prados E F, Seriacopi V, Fukumasu N K, Lima L G D S, Machado I F, Souza R M. Numerical modeling of adhesion and adhesive failure during unidirectional contact between metallic surfaces. *Friction* **4**(3): 217–227 (2016)
[41] Varshney V, Patnaik S S, Muratore C, Roy A K, Voevodin A A, FarmerB L. MD simulations of molybdenum disulphide (MoS_2): Force-field parameterization and thermal transport behavior. *Comput Mater Sci* **48**(1): 101–108 (2010)
[42] Yang Y, Devel M, Wang Z. An atomistic model for the charge distribution in layered MoS_2. *J Chem Phys* **149**(12): 124102 (2018)
[43] Wang Z. Effects of substrate and electric fields on charges in nanotubes. *Phys Rev B* **79**(15): 155407 (2009)
[44] Steiner P, Roth R, Gnecco E, Baratoff A, Maier S, Glatzel T, Meyer E. Two-dimensional simulation of superlubricity on NaCl and highly oriented pyrolytic graphite. *Phys Rev B* **79**(4): 045414 (2009)
[45] Donnet C, Martin J M, LeMogne T, Belin M. Super-low friction of MoS_2 coatings in various environments. *Tribol Int* **29**(2): 123–128 (1996)
[46] Wang Z. Chirality-dependent motion transmission between aligned carbon nanotubes. *Carbon* **151**: 130–135 (2019)
[47] Hölscher H, Ebeling D, Schwarz U D. Friction at atomic-scale surface steps: Experiment and theory. *Phys Rev Lett* **101**(24): 246105 (2008)
[48] Miura K, Kamiya S. Observation of the Amontons-Coulomb law on the nanoscale: Frictional forces between MoS_2 flakes and MoS_2 surfaces. *Eur Phys Lett* **58**(4): 610 (2002)

[49] Zeng X, Peng Y, Lang H, Yu K. Probing the difference in friction performance between graphene and MoS_2 by manipulating the silver nanowires. *J Mater Sci* **54**(1): 540–551 (2019)
[50] Wang Z. Chirality-selective transport of benzene molecules on carbon nanotubes. *J Phys Chem C* **124**(6): 3851–3856 (2020)
[51] Wang Z. Gear junctions between chiral boron nitride nanotubes. *Phys Rev B* **100**(3): 035430 (2019)

Shengcong WU. He received his bachelor degree in applied physics in 2017 from Jiangsu University of Science and Technology, Zhenjiang, China. Then, he was a master student in the Guangxi Key Laboratory for Relativistic Astrophysics at Guangxi University. He has recently obtained his master degree in Department of Physics at Guangxi University. His research interests include structural superlubricity of nanomaterials.

Zhao WANG. He received his Ph.D. degree in physics at the University of Besancon in France. He has been working at EMPA in Thun (Switzerland) and CEA in Grenoble (France) as a postdoc after graduation. He came back to China in 2011, for working at Xi'an Jiaotong University. He joined Guangxi University since 2016 as a professor. His research concentrates on molecular physics, as well as on mechanical and thermal transport properties of nanoscale interfaces.